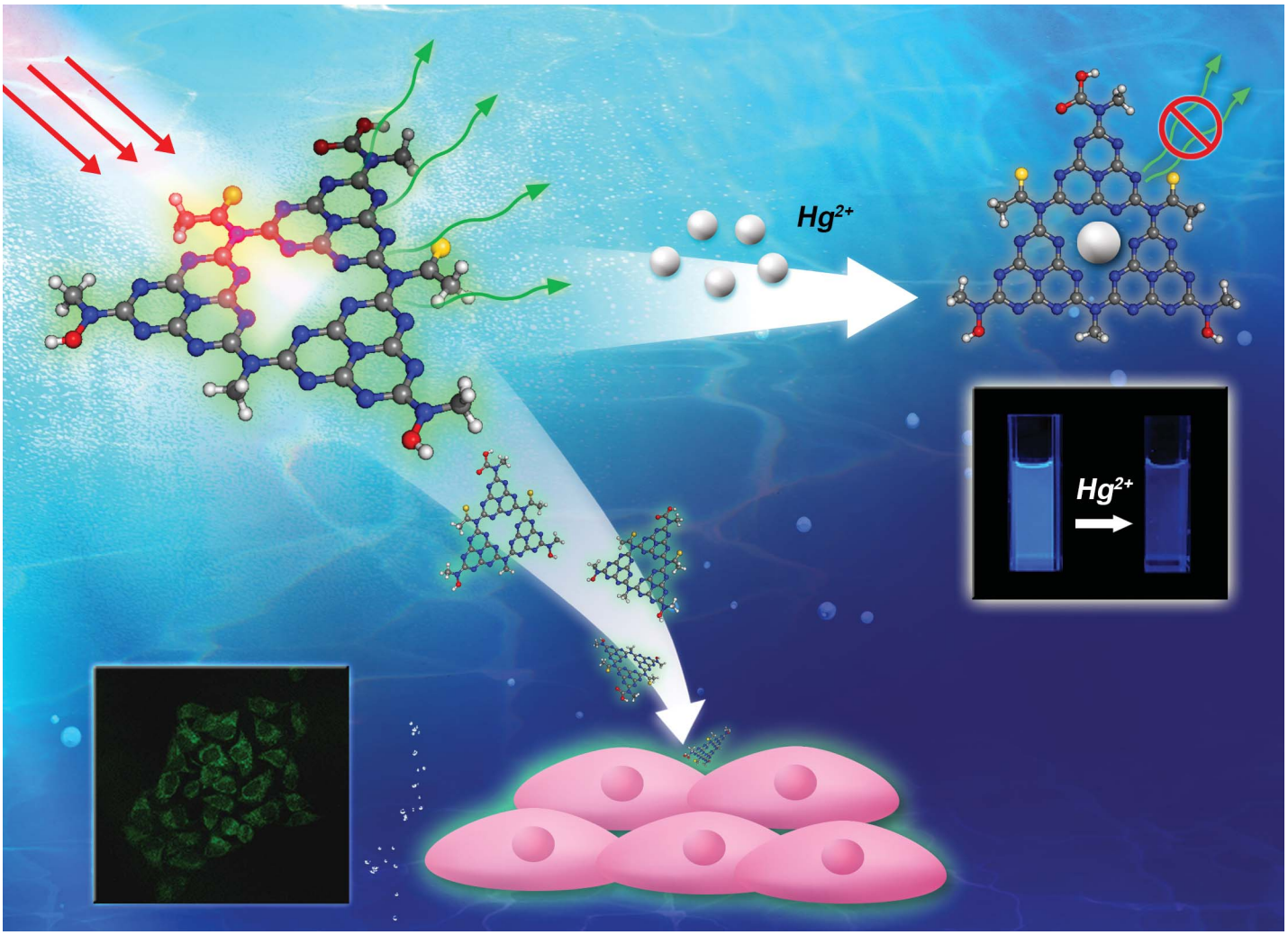

Highlighting work on oxygen and sulfur co-doped graphitic carbon nitride fluorescent quantum dots presented by Prof. Jiu-Ju Feng, Dr. Linxiang Shao and co-workers at College of Chemistry and Life Science, Zhejiang Normal University, Jinhua, China.

Title: Facile synthesis of oxygen and sulfur co-doped graphitic carbon nitride fluorescent quantum dots and their application for mercury(II) detection and bioimaging

Oxygen and sulfur co-doped graphitic carbon nitride fluorescent quantum dots were prepared by a simple and facile thermal-treatment of citric acid and thiourea. The as-prepared products showed bright blue photoluminescence, which exhibited improved selectivity and sensitivity for Hg^{2+} detection, along with enhanced biocompatibility and lower cytotoxicity for cell imaging.

As featured in:

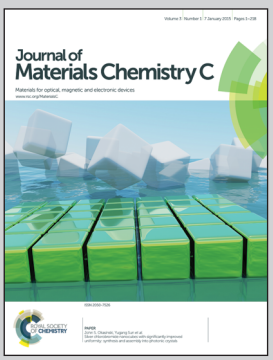

See Jiu-Ju Feng, Linxiang Shao *et al.*, *J. Mater. Chem. C*, 2015, **3**, 73.

ROYAL SOCIETY OF CHEMISTRY

www.rsc.org/MaterialsC

Registered charity number: 207890

Journal of Materials Chemistry C

PAPER

View Article Online
View Journal | View Issue

Cite this: J. Mater. Chem. C, 2015, 3, 73

Facile synthesis of oxygen and sulfur co-doped graphitic carbon nitride fluorescent quantum dots and their application for mercury(II) detection and bioimaging†

Ya-Chun Lu,‡[a] Jia Chen,‡[a] Ai-Jun Wang,[a] Ning Bao,[b] Jiu-Ju Feng,*[a] Weiping Wang[a] and Linxiang Shao*[a]

Received 19th September 2014
Accepted 28th October 2014

DOI: 10.1039/c4tc02111h

www.rsc.org/MaterialsC

In this work, uniform oxygen and sulfur co-doped graphitic carbon nitride quantum dots (OS-GCNQDs) have been prepared by thermal treatment of citric acid and thiourea. The as-obtained OS-GCNQDs show strong blue photoluminescence (PL) with a relatively high quantum yield of 14.5%. Furthermore, OS-GCNQDs exhibit stable and specific concentration-dependent PL intensities in the presence of mercury(II) ions in the range of 0.001–20.0 μM, with a detection limit of 0.37 nM (3*S*/*N*). More importantly, OS-GCNQDs were explored for cell imaging with satisfactory biocompatibility, and so are a potential fluorescent probe in biosensing and bioimaging applications.

Introduction

Carbon quantum dots (CQDs) have received growing research interest as promising carbon materials since they were discovered in 2004.[1] Recently, many efforts have been focused on their prospective applications in optoelectronic devices,[2] photocatalysis,[3] electrocatalysis,[4] biosensing, and bioimaging,[5–7] owing to their superior properties, such as bright luminescence, good biocompatibility, and low toxicity.[8,9] Specifically, their potential applications in the biological field are keenly anticipated. Therefore, intensive investigations have been carried out and numerous synthetic methods developed,[10–12] such as electrochemical oxidation,[13] ultrasonic treatment,[14] microwave methods,[15] solid thermal treatment,[16] and hydrothermal methods.[17]

Now, CQDs have broad applications in biochemical assays. Chen *et al.* synthesized CQDs from oil acid for cell imaging.[18] Zhang's group fabricated CQDs *via* the oxidation of activated carbon by nitric acid. They also demonstrated selective and sensitive responses of CQDs to Cu^{2+}.[19] However, un-doped CQDs might have the disadvantage of self-quenching, thereby limit their further applications in bioanalysis.[20] This is due to the intra-molecular ground-state dimer complex or energy transfer between the adjacent CQDs.

Alternatively, doped CQDs can almost retain all the advantages of blank CQDs and further avoid self-quenching phenomenon because of their substantial ensemble Stokes shift. Therefore, many researchers have paid much attention to doped CQDs with heteroatoms, especially nitrogen and sulfur.[21–23] For cell imaging, our group synthesized N-doped CQDs (N-CQDs) by a thermal route from streptomycin.[24] We also developed a solvent-free synthesis method to prepare SN-CQDs from glutathione for a highly selective and sensitive detection for mercury(II) ions.[25] It needs to be emphasized that graphitic carbon nitride quantum dots (GNCQDs) are unique among heteroatom-doped CQDs as their structures are similar to graphene. They have broad applications in biomass conversion and sustainable chemistry, due to their functional groups.[16,26,27]

The mercury(II) ion (Hg^{2+}) is one of the heavy metal ions widely used in industry and agriculture.[28] Its strong toxicity and bioaccumulation result in serious human health problems even at very low concentrations.[29] Therefore, developing a novel method for the trace detection of Hg^{2+} is very important. Conventional analytical approaches include atomic absorption/emission spectroscopy,[30,31] Auger-electron spectroscopy,[32] inductively coupled plasma mass spectrometry,[33] ultraviolet-visible spectrometry,[34] and polarography.[35]

In this work, we developed a facile one-step route for the synthesis of OS-GNCQDs from citric acid and thiourea (Scheme 1). The optical properties of the as-prepared OS-GNCQDs were examined in detail. Furthermore, OS-GNCQDs were explored for the selective and sensitive detection of Hg^{2+} as a model system.

[a]*College of Chemistry and Life Science, College of Geography and Environmental Science, Zhejiang Normal University, Jinhua 321004, China. E-mail: jjfeng@zjnu.cn; shaolinxiang@zjnu.cn; Fax: +86-579-82282269; Tel: +86-579-82282269*

[b]*School of Public Health, Nantong University, Nantong 226019, China*

† Electronic supplementary information (ESI) available. See DOI: 10.1039/c4tc02111h

‡ These authors contributed equally to this work.

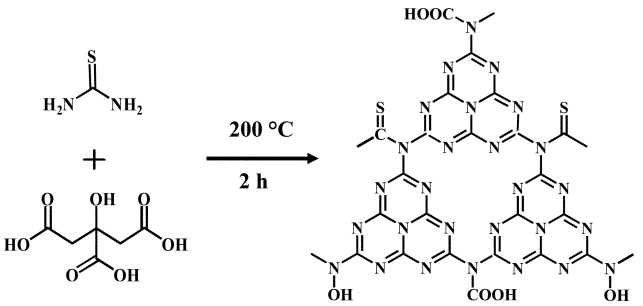

Scheme 1 Formation mechanism of highly fluorescent OS-GNCQDs.

Experimental

Materials

Citric acid and thiourea were purchased from Sinopharm Chemical Reagent Co., Ltd. (Shanghai, China). Mercuric nitrate, sodium nitrate, zinc sulfate heptahydrate, silver nitrate, manganese acetate tetrahydrate, copper nitrate trihydrate, nickel chloride hexahydrate, anhydrous magnesium sulfate, barium nitrate, aluminum nitrate nonahydrate, calcium nitrate tetrahydrate, cadmium chloride hemi(pentahydrate), ferric chloride, potassium chloride, iron(II) chloride tetrahydrate, and lead nitrate were received from Aladdin Chemistry Reagent Company (Shanghai, China). All the other chemicals were analytical grade and used as received. Twice-distilled water was used throughout all the experiments.

Preparation of OS-GNCQDs

In a typical preparation of OS-GNCQDs (Scheme 1), 0.21 g citric acid and 0.23 g thiourea were mixed together under stirring (Fig. S1, ESI†). Next, the mixture was put into a 50 mL Teflon-lined autoclave, heated at 200 °C for 2.0 h (Fig. S2, ESI†), and cooled to room temperature in air. The product was dissolved with water, and re-purified with a 0.22 μM filter membrane to discard the nonfluorescent deposits, which were large particles with a flake-like structure. (Fig. S3, ESI†). The supernatant was collected and further diluted to prepare OS-GNCQD suspensions (5.0 mg mL^{-1}).

Instruments

UV-vis absorption spectra of the samples were recorded on a Lambda 950 UV-vis spectrophotometer (Perkin-Elmer, USA). Fluorescence emission spectroscopy was carried out on a LS-45 fluorescence spectrophotometer (Perkin-Elmer, UK). X-ray diffraction (XRD) measurements were performed on a Philips PW3040/60 automatic powder diffractometer using Cu Kα radiation. Fourier transform infrared spectra (FT-IR) were recorded on a Nicolet 670 FT-IR spectrometer in the form of KBr pellets. Transmission electron microscopy (TEM) and high resolution TEM (HR-TEM) images were taken on a JEOL-2100F transmission electron microscope. X-ray photoelectron spectra (XPS) were acquired on a Themo SCIENTIFIC ESCALAB 250 spectrometer with Al Kα X-ray radiation (1486.6 eV).

Fluorescence detection of Hg^{2+}

For a typical assay, 5.0 μL of OS-GNCQD suspension (5.0 mg mL^{-1}) were diluted with 3.0 mL of water, followed by the addition of different concentrations of Hg^{2+}. The mixed solutions were kept static, reacted for 20 min, and finally the associated fluorescence quenching spectra with an excitation wavelength of 369 nm were recorded at room temperature.

Selectivity and interference measurements

The selectivity of OS-GNCQDs was examined using some interfering compounds such as Ag^{+}, Al^{3+}, Cd^{2+}, Co^{2+}, Cu^{2+}, Fe^{2+}, Fe^{3+}, Mg^{2+}, Mn^{2+}, Na^{+}, Ni^{2+}, Pb^{2+}, and Zn^{2+} under identical conditions. The concentrations of Hg^{2+} and the interferent ions were all 50.0 μM. For studying the interference, the OS-GNCQD suspension was mixed with Hg^{2+} in the absence and presence of other interferent chemicals at concentrations four times that of Hg^{2+}. The associated fluorescence spectra were quickly recorded after incubation for 20 min.

Cell imaging and toxicity assay

The cytotoxicity of OS-GNCQDs to human umbilical vein endothelial cells (HUVEC) was evaluated by a standard methylthiazolydiphenyltetrazolium bromide (MTT) assay. HUVEC were seeded in 96-well U-bottom plates at a density of 5.0×10^4–1.0×10^5 cells per milliliter (90.0 μL per well) and were initially cultured for 12 h in an incubator (37 °C, 5% CO_2), prior to the addition of the OS-GNCQD suspension at a range of concentrations. After being cultured for a further 24 h with OS-GNCQDs, 20.0 μL of MTT solution (normal saline or 1.0 mg mL^{-1} phosphate buffer solution) was added to each sample, and incubated at 37 °C for 4 h. The culture media were discarded; then, 150.0 μL dimethylsulfoxide (DMSO) was added to each sample in order to dissolve the formazan, with shaking for at least 15 min. The corresponding spectra were recorded with a microplate reader at 570 nm. The cell viability rate (VR) was calculated based on the below equation:

$$\mathrm{VR}\ (\%) = A/A_0 \times 100\%$$

where A is the absorbance of the experimental group (the cells treated with the OS-GNCQD suspensions) and A_0 is the absorbance of the control group.

Results and discussion

Fig. 1 shows the optical properties of OS-GNCQDs. Specifically, there is a UV-vis absorption peak centered at 338 nm, implying the presence of carbonyl or conjugated carbonyl groups. At the same time, the excitation and emission peaks appeared at 369 and 444 nm, respectively. In addition, the OS-GNCQD suspension exhibits a yellow color under visible light, whereas it is blue upon excitation with UV light of 365 nm (insets in Fig. 1A).

As illustrated in Fig. 1B, the fluorescence spectra of the OS-GNCQDs shows a red shift by adjusting the excitation wavelength from 369 to 415 nm, accompanied by a fast decrease of the PL intensities. This indicates the excitation-dependent

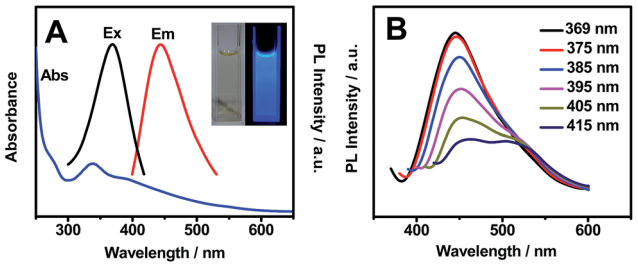

Fig. 1 (A) Absorbance, excitation, and emission spectra of OS-GNCQDs. (B) The excitation-dependent emission spectra of OS-GNCQDs. Insets show the corresponding photographs taken under visible light (left) and UV light of 365 nm (right).

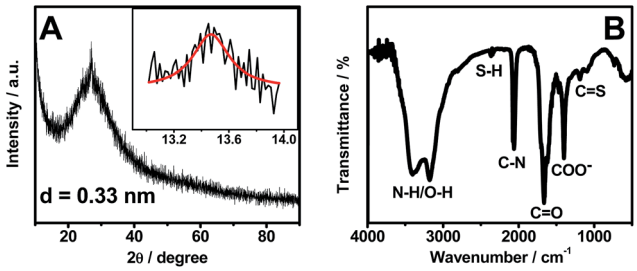

Fig. 3 XRD pattern (A) and FT-IR spectrum (B) of OS-GNCQDs.

emission behavior of OS-GNCQDs, as supported by previous reports.[7,18] Meanwhile, using quinine sulfate (54% in 0.1 mol L^{-1} H_2SO_4, λ_{ex} = 369 nm) as a reference, the fluorescence quantum yield was calculated to be about 14.5% for OS-GNCQDs. This value is comparable to CQDs prepared from Bombyx mori silk,[36] soya bean grounds,[37] and ionic liquids,[38] and fully consistent with previous research in which hetero-atom-doped CQDs was found to enhance fluorescence dramatically.[20,39]

As shown by TEM images (Fig. 2), OS-GNCQDs have spherical shapes with an average size of 2.78 nm, similar to previous findings.[3] Furthermore, well-defined lattice fringes are clearly observed (inset in Fig. 2A), with an inter-fringe distance of 0.202 nm, corresponding to the (102) diffraction planes of graphitic (sp^2) carbon.[40] This value matches well with CQDs using pemelo peel[40] and natural gas soot[41] as carbon sources. Fig. 2B reveals the narrow size distribution of OS-GNCQDs, with an average size of 2.75 nm.

As displayed in Fig. 3A, there is a broad peak located at 27.0° and a weak one at 13.4° in the XRD pattern of OS-GNCQDs. The former represents the inter-planar graphitic stacking, and the latter is indicative of in-plane structural packing, reflecting the formation of graphitic carbon nitride.[42,43]

Meanwhile, FT-IR analysis was carried out to characterize the surface groups of OS-GNCQDs (Fig. 3B). The peaks emerge at 3415 and 3175 cm^{-1}, which correspond to the stretching modes of N–H/O–H, suggesting highly hydrophilic property of OS-GNCQDs.[3] The peak of 2380 cm^{-1} is ascribed to the stretching vibration of the S–H group, 2070 cm^{-1} to the C–N group,[23] 1670 cm^{-1} to the vibration absorption of C=O in COOH, 1410 cm^{-1} to the COO^- group, and 1180–1080 cm^{-1} to C=S vibrations.[3,23] These results illustrate OS-GNCQDs with desirable functional groups.

As revealed by the survey XPS spectrum of NSCDs (Fig. 4A), the typical product mainly contains O, N, C, S, and S elements. Specifically, the high-resolution C_{1s} spectrum (Fig. 4B) shows five peaks detected at 284.2, 284.7, 285.3, 287.7, and 288.6 eV, which are attributed to C=C, C–C/C–H, C–OH/C–O–C, C=O, and COOH groups, respectively.[44] And there are two peaks located at 398.9 and 399.6 eV in the high-resolution N_{1s} region (Fig. 4C), which arise from pyridinic N and pyrrolic N,[11] respectively. Similarly, two peaks emerge at 530.8 and 531.7 eV for the O_{1s} spectrum (Fig. S4, ESI†), which originate from C–O and C=O bands,[45] respectively. Additionally, seven peaks are detected in the S_{2p} spectrum (Fig. 4D), corresponding to –SH (161.8 eV), C–S_n–C (n = 1 or 2, 163.5 eV), –C=S– (164.8 eV), sulfoxide (166.2 eV), and –C–SO_x– (x = 2, 167.7 eV; 3, 168.5 eV; 4, 169.3 eV),[23,46] respectively. These phenomena demonstrate the formation of OS-GNCQDs in the present work.

Fig. S5 (ESI†) illustrates the effects of pH values and salinity of the solutions on the PL intensities of OS-GNCQDs. The results verify a good stability of OS-GNCQDs in different physiological environments. Besides, OS-GNCQDs exhibit better

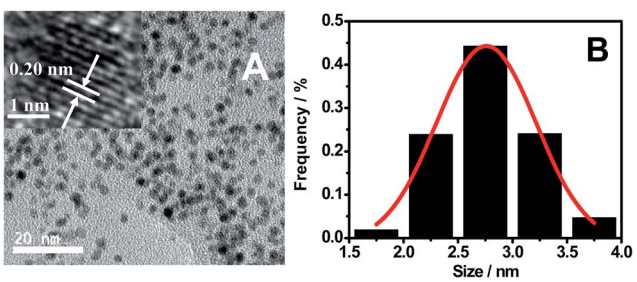

Fig. 2 TEM image (A) and the respective size distribution (B) measured for 400 nanodots randomly. Inset shows high-resolution TEM image of an individual nanodot.

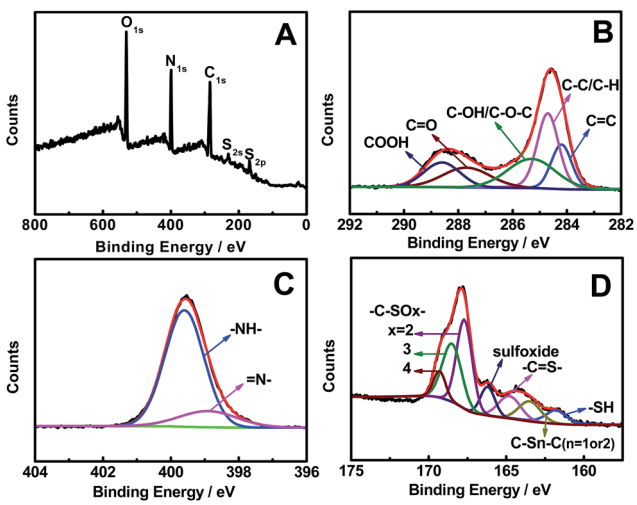

Fig. 4 Survey (A), high-resolution C_{1s} (B), N_{1s} (C), and S_{2p} (D) XPS spectra of OS-GNCQDs.

photostability than traditional organic dyes such as rhodamine 6G. After three months storage at room temperature, OS-GNCQDs remain similar in PL intensity. These properties make OS-GNCQDs a potential fluorescent probe for biosensing and bioimaging.

To estimate the selectivity of OS-GNCQDs as a fluorescent probe, the PL intensities of OS-GNCQDs were analyzed in the presence of metal ions at a concentration of 50.0 μM (Fig. 5A). It is found that fluorescence responses of OS-GNCQDs are different in the presence of different metal ions even under the same conditions. Impressively, the PL intensity of OS-GNCQDs can be greatly quenched in the case of Hg^{2+}. Based on this phenomenon, OS-GNCQDs were efficiently used for the selective detection of Hg^{2+} in coexistence with other metal ions at a concentration of 200.0 μM (Fig. 5B). The outstanding selectivity and specificity can be ascribed to the stronger affinity of Hg^{2+} to amino groups and thiourea groups on the surface of OS-GNCQDs, relative to the affinities of other metal ions.

Fig. 6 shows the changes in high-resolution N and S spectra of OS-GNCQDs before and after the addition of Hg^{2+}. The peak of N_{1s} at 399.0 eV greatly decreases (Fig. 6A). This clearly demonstrates that Hg^{2+} has strong interactions with the pyridine nitrogen in OS-GNCQDs, which generate energy transfer from the OS-GNCQDs to Hg^{2+}, leading to fluorescence quenching. Moreover, the sulfur peak at 162.6 eV significantly increases and the peak at 168.0 eV obviously decreases (Fig. 6B). This is ascribed to the formation of –C=S–Hg complexes based on the high affinity of thiourea groups to Hg^{2+}. The as-formed complexes can facilitate electron transfer and restrain the radioactive recombination of excitations, leading to remarkable quenching effects on fluorescence intensity.[47]

In addition, the PL lifetime of OS-GNCQDs is measured to be 7.88 ns, with excitation and emission wavelengths of 369 and 444 nm, respectively (Fig. 7). Nevertheless, the respective lifetime is decreased to 7.70 ns after the addition of Hg^{2+}, mainly due to the static quenching that occurs in this case. Furthermore, this value is equal to that of CQDs prepared from streptomycin.[24] This means that OS-GNCQDs can be used as a promising probe in biological analysis.

As described in Fig. 8, the PL intensities of OS-GNCQDs linearly decrease with Hg^{2+} concentrations. The quenching efficiency can be well fitted by the following Stern–Volmer equation:

$$F_0/F = 1 + K_{sv}Q,$$

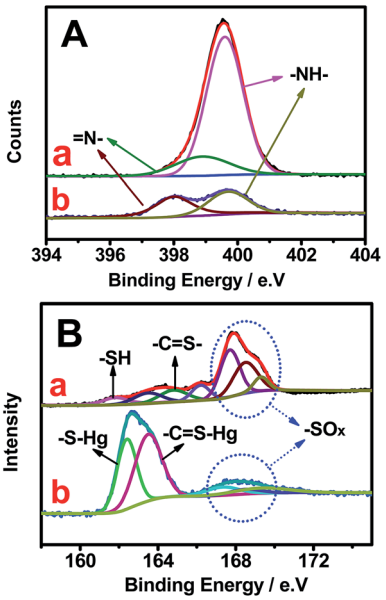

Fig. 6 High-resolution N_{1s} (A) and S_{2p} (B) XPS spectra of OS-GCNQDs before (a) and after (b) the addition of Hg^{2+}.

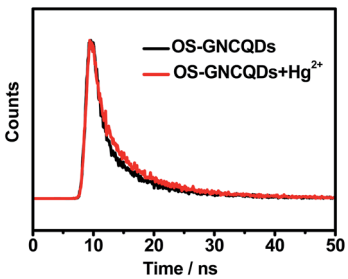

Fig. 7 Fluorescence decay trace of OS-GCNQDs upon excitation at 369 nm.

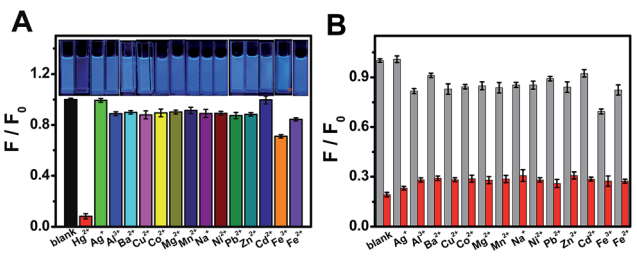

Fig. 5 (A) Fluorescence responses of OS-GNCQDs in the presence of different metal ions (λ_{ex} = 369 nm; $[M^{n+}]$ = 50.0 μM). The inset displays the photographs in accordance with the spectra. (B) The relative fluorescence intensities (F/F_0) of OS-GCNQDs in the presence of metal ions (200.0 μM), and following treatment of the mixture solution with 50.0 μM Hg^{2+} (red column).

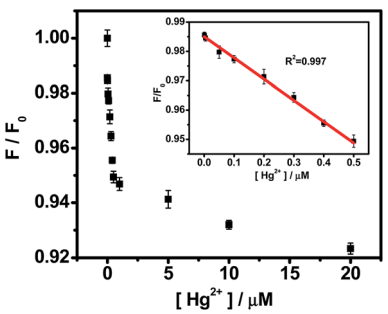

Fig. 8 The relationship of the F/F_0 and Hg^{2+} concentrations. The inset shows the linear range of 0.001–0.5 μM. The error bars represent variations among three independent measurements.

where F_0 and F are the PL intensities of OS-GNCQDs in the absence and presence of Hg^{2+}, respectively, Q is the concentration of Hg^{2+}, and K_{sv} is the Stern–Volmer constant.

Specifically, the PL intensities show linear responses to Hg^{2+} concentrations in the range of 0.001–0.5 μM (inset in Fig. 8). The detection limit is about 0.37 nM ($S/N = 3$) for Hg^{2+} detection. OS-GNCQDs have good sensitivity and a wide linear range, in contrast to those given in the literature, as listed in Table S1 (ESI†). The superior selectivity and sensitivity make OS-GNCQD a promising fluorescent probe in biomedical and environmental systems.

The MTT assay was conducted with HUVEC as a model cell to test the cytotoxicity of OS-GNCQDs, since cancer cells usually have more resistance to most chemical compounds. As depicted in Fig. 9, OS-GNCQDs exhibit good biocompatibility and low cytotoxicity for HUVEC, revealing a possible application of OS-GNCQDs for cell imaging.

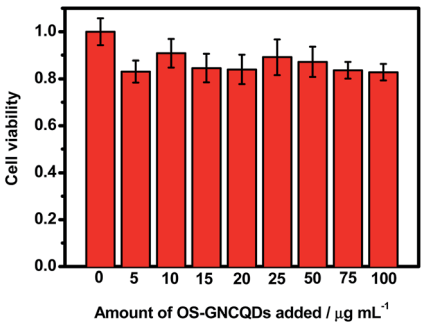

Fig. 9 Cell viability assays of HUVEC treated with different concentrations of OS-GNCQDs.

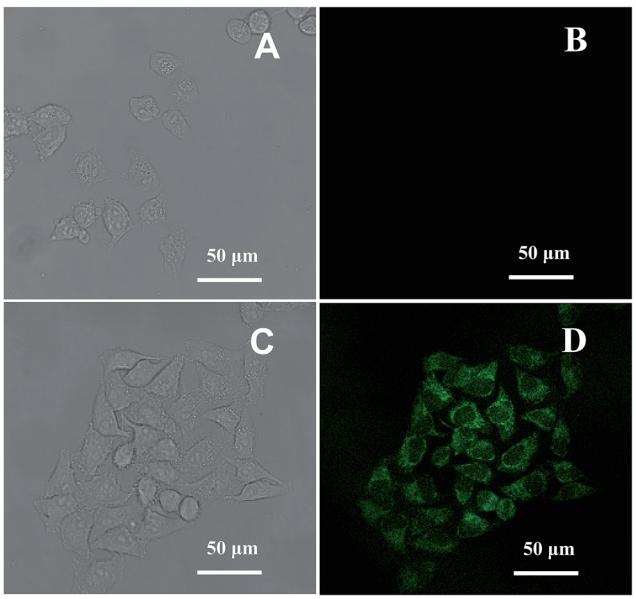

Fig. 10 Images of HeLa cells in the absence (A and B) and presence (C and D) of OS-GNCQDs taken under bright field (A and C) and at an excitation wavelength of 488 nm (B and D) with 75.0 μg mL^{-1} of OS-GNCQDs.

Fig. 10 shows confocal images of HeLa cells treated with OS-GNCQDs (75.0 μg mL^{-1}). The fluorescence becomes brighter with the increase of the CQD concentrations, and *vice versa* (Fig. S6, ESI†). It is noteworthy that the concentration of OS-GNCQDs (75.0 μg mL^{-1}) is much higher and the incubation time (24 h) is much longer for *in vitro* evaluation. These results indicate the better biocompatibility of OS-GNCQDs, which can be used for *in vivo* applications such as bioimaging.

Before incubation of HeLa cells with OS-GNCQD solution, there is no fluorescent response at a wavelength of 488 nm (Fig. 10A and B). After incubation, the cells in the cytoplasm become bright green under excitation at 488 nm. This means that CQDs can easily penetrate into the cytoplasm and label the cells simultaneously, illustrating the greatly improved fluorescence performance of OS-GNCQDs as a fluorescent probe in bioimaging.[24,43,44] Therefore, OS-GNCQDs can potentially be applied for the investigation of labeled cytoplasm.

Conclusion

In summary, we report a simple route for synthesis of water-soluble OS-GNCQDs by a thermal treatment of citric acid and thiourea. The as-prepared uniform OS-GNCQDs possess a quantum yield of 14.5%, and have an average size of 2.78 nm, which is used for the selective and sensitive detection of Hg^{2+} with a detection limit of 0.37 nM. Furthermore, OS-GNCQDs were explored for bioimaging with improved biocompatibility.

Acknowledgements

This work was financially supported by National Natural Science Foundation of China (nos 21475118, 21175118, 21275130, 21305128 and 21345006), and Zhejiang province university young academic leaders of academic climbing project (no pd2013055).

References

1 X. Xu, R. Ray, Y. Gu, H. J. Ploehn, L. Gearheart, K. Raker and W. A. Scrivens, *J. Am. Chem. Soc.*, 2004, **126**, 12736–12737.
2 D. Zhang, Y. Hao, L. Zheng, Y. Ma, H. Feng and H. Luo, *J. Mater. Chem. A*, 2013, **1**, 7584–7591.
3 D. Qu, M. Zheng, P. Du, L. Zhang, Y. Zhou, D. Li, H. Tan, Z. Zhao, Z. Xie and Z. Sun, *Nanoscale*, 2013, **5**, 12272–12277.
4 Z. Liu, H. Nie, Z. Yang, J. Zhang, Z. Jin, Y. Lu, Z. Xiao and S. Huang, *Nanoscale*, 2013, **5**, 3283–3288.
5 K. Qu, J. Wang, J. Ren and X. Qu, *Chem.–Eur. J.*, 2013, **19**, 7243–7249.
6 A. Salinas-Castillo, M. Ariza-Avidad, C. Pritz, M. Camprubi-Robles, B. Fernandez, M. J. Ruedas-Rama, A. Megia-Fernandez, A. Lapresta-Fernandez, F. Santoyo-Gonzalez, A. Schrott-Fischer and L. F. Capitan-Vallvey, *Chem. Commun.*, 2013, **49**, 1103–1105.
7 L. Shen, L. Zhang, M. Chen, X. Chen and J. Wang, *Carbon*, 2013, **55**, 343–349.
8 J. C. G. Esteves da Silva and H. M. R. Gonçalves, *Trends Anal. Chem.*, 2011, **30**, 1327–1336.

9 P. G. Luo, S. Sahu, S.-T. Yang, S. K. Sonkar, J. Wang, H. Wang, G. E. LeCroy, L. Cao and Y.-P. Sun, *J. Mater. Chem. B*, 2013, **1**, 2116–2127.
10 M. Tan, L. Zhang, R. Tang, X. Song, Y. Li, H. Wu, Y. Wang, G. Lv, W. Liu and X. Ma, *Talanta*, 2013, **115**, 950–956.
11 Z. Qian, J. Ma, X. Shan, L. Shao, J. Zhou, J. Chen and H. Feng, *RSC Adv.*, 2013, **3**, 14571–14579.
12 X. Wang, K. Qu, B. Xu, J. Ren and X. Qu, *Nano Res.*, 2011, **4**, 908–920.
13 Y.-L. Zhang, L. Wang, H.-C. Zhang, Y. Liu, H.-Y. Wang, Z.-H. Kang and S.-T. Lee, *RSC Adv.*, 2013, **3**, 3733–3738.
14 S. Zhuo, M. Shao and S.-T. Lee, *ACS Nano*, 2012, **6**, 1059–1064.
15 Y. Liu, N. Xiao, N. Gong, H. Wang, X. Shi, W. Gu and L. Ye, *Carbon*, 2014, **68**, 258–264.
16 J. Zhou, Y. Yang and C.-Y. Zhang, *Chem. Commun.*, 2013, **49**, 8605–8607.
17 W. Li, Z. Zhang, B. Kong, S. Feng, J. Wang, L. Wang, J. Yang, F. Zhang, P. Wu and D. Zhao, *Angew. Chem., Int. Ed.*, 2013, **52**, 1–6.
18 B. Chen, F. Li, S. Li, W. Weng, H. Guo, T. Guo, X. Zhang, Y. Chen, T. Huang, X. Hong, S. You, Y. Lin, K. Zeng and S. Chen, *Nanoscale*, 2013, **5**, 1967–1971.
19 S. Zhang, Q. Wang, G. Tian and H. Ge, *Mater. Lett.*, 2014, **115**, 233–236.
20 P. Wu and X.-P. Yan, *Chem. Soc. Rev.*, 2013, **42**, 5489–5521.
21 W. Shi, X. Li and H. Ma, *Angew. Chem.*, 2012, **124**, 6538–6541.
22 S. Chandra, P. Patra, S. H. Pathan, S. Roy, S. Mitra, A. Layek, R. Bhar, P. Pramanik and A. Goswami, *J. Mater. Chem. B*, 2013, **1**, 2375–2382.
23 D. Sun, R. Ban, P.-H. Zhang, G.-H. Wu, J.-R. Zhang and J.-J. Zhu, *Carbon*, 2013, **64**, 424–434.
24 W. Wang, Y.-C. Lu, H. Huang, J.-J. Feng, J.-R. Chen and A.-J. Wang, *Analyst*, 2014, **139**, 1692–1696.
25 W. Wang, Y.-C. Lu, H. Huang, A.-J. Wang, J.-R. Chen and J.-J. Feng, *Sens. Actuators, B*, 2014, **202**, 741–747.
26 Y. Wang, X. Wang and M. Antonietti, *Angew. Chem., Int. Ed.*, 2012, **51**, 68–89.
27 Y. Zhang, J. Liu, G. Wu and W. Chen, *Nanoscale*, 2012, **4**, 5300–5303.
28 R. Liu, H. Li, W. Kong, J. Liu, Y. Liu, C. Tong, X. Zhang and Z. Kang, *Mater. Res. Bull.*, 2013, **48**, 2529–2534.
29 R. Zhang and W. Chen, *Biosens. Bioelectron.*, 2014, **55**, 83–90.
30 J. Margetínová, P. Houserová-Pelcová and V. Kubáň, *Anal. Chim. Acta*, 2008, **615**, 115–123.
31 S. Gil, I. Lavilla and C. Bendicho, *Spectrochim. Acta B*, 2007, **62**, 69–75.
32 M. Miró and E. H. Hansen, *Anal. Chim. Acta*, 2013, **782**, 1–11.
33 A. Castillo, A. F. Roig-Navarro and O. J. Pozo, *Anal. Chim. Acta*, 2006, **577**, 18–25.
34 H. Bagheri and A. Gholami, *Talanta*, 2001, **55**, 1141–1150.
35 S. Z. Milić, N. I. Potkonjak, S. Ž. Gorjanović, S. D. Veljović-Jovanović, F. T. Pastor and D. Ž. Sužnjević, *Electroanalysis*, 2011, **23**, 2935–2940.
36 Z. L. Wu, P. Zhang, M. X. Gao, C. F. Liu, W. Wang, F. Leng and C. Z. Huang, *J. Mater. Chem. B*, 2013, **1**, 2868–2873.
37 W. Li, Z. Yue, C. Wang, W. Zhang and G. Liu, *RSC Adv.*, 2013, **3**, 20662–20665.
38 A. Zhao, C. Zhao, M. Li, J. Ren and X. Qu, *Anal. Chim. Acta*, 2014, **809**, 128–133.
39 C. Liu, P. Zhang, F. Tian, W. Li, F. Li and W. Liu, *J. Mater. Chem.*, 2011, **21**, 13163–13167.
40 W. Lu, X. Qin, S. Liu, G. Chang, Y. Zhang, Y. Luo, A. M. Asiri, A. O. Al-Youbi and X. Sun, *Anal. Chem.*, 2012, **84**, 5351–5357.
41 L. Tian, D. Ghosh, W. Chen, S. Pradhan, X. Chang and S. Chen, *Chem. Mater.*, 2009, **21**, 2803–2809.
42 Q. Su, J. Sun, J. Wang, Z. Yang, W. Cheng and S. Zhang, *Catal. Sci. Technol*, 2014, **4**, 1556–1562.
43 G. Zhang, J. Zhang, M. Zhang and X. Wang, *J. Mater. Chem.*, 2012, **22**, 8083–8091.
44 S. Sahu, B. Behera, T. K. Maiti and S. Mohapatra, *Chem. Commun.*, 2012, **48**, 8835–8837.
45 J. Wei, J. Shen, X. Zhang, S. Guo, J. Pan, X. Hou, H. Zhang, L. Wang and B. Feng, *RSC Adv.*, 2013, **3**, 13119–13122.
46 Y. Su, Y. Zhang, X. Zhuang, S. Li, D. Wu, F. Zhang and X. Feng, *Carbon*, 2013, **62**, 296–301.
47 H. Huang, J.-J. Lv, D.-L. Zhou, N. Bao, Y. Xu, A.-J. Wang and J.-J. Feng, *RSC Adv.*, 2013, **3**, 21691–21696.

